Check for updates

Received: 1 September 2020 | Revised: 25 March 2021 | Accepted: 20 April 2021

DOI: 10.1111/jace.17877

Journal of the American Ceramic Society

ORIGINAL ARTICLE

# Structure and viscosity of $CaO–Al_2O_3–B_2O_3–BaO$ slags with varying mass ratio of BaO to CaO

**Harishchandra Singh[1] | Qifeng Shu[2,3] | Graham King[4] | Ziqing Liang[3] | Zhifeng Wang[3] | Wei Cao[1] | Marko Huttula[1,5] | Timo Fabritius[2]**

[1]Nano and Molecular Systems Research Unit, University of Oulu, Oulu, Finland

[2]Research Unit of Process Metallurgy, University of Oulu, Oulu, Finland

[3]School of Metallurgical and Ecological Engineering, University of Science and Technology, Beijing, China

[4]Canadian Light Source, Saskatoon, Saskatchewan, Canada

[5]School of Materials Science and Engineering, Henan University of Science and Technology, Luoyang, Henan, China

**Correspondence**
Qifeng Shu, Research unit of process metallurgy, University of Oulu, Oulu, Finland.
Emails: qifeng.shu@oulu.fi, shuqifeng@gmail.com

**Funding information**
Academy of Finland, Grant/Award Number: 311934; National Natural Science Foundation of China, Grant/Award Number: 51774026

**Abstract**

The structure of $CaO–Al_2O_3–B_2O_3–BaO$ glassy slags with varying mass ratio of BaO to CaO has been investigated by Raman spectroscopy, $^{11}B$ and $^{27}Al$ magic angle spinning nuclear magnetic resonance (MAS-NMR) spectroscopy and atomic pair distribution function (PDF). $^{11}B$ MAS-NMR spectra reveal the dominant coordination of boron as trigonal. Both simulations on $^{11}B$ MAS-NMR spectra and Raman spectroscopy indicate the presence of orthoborate as the primary borate group with a few borate groups with one bridging oxygen and minor four-coordinated boron sites. $^{27}Al$ MAS-NMR and PDF show the Al coordination as tetrahedral. Raman spectral study shows that the transverse vibration of $Al^{IV}–O–Al^{IV}$ and $Al^{IV}–O–B^{III}$, stretching vibration of aluminate structural units and vibration of orthoborate and pyroborate structural groups. A broader distribution of Al–O bond lengths in PDF also supports the enhanced network connectivity. Viscosity measurements show the increase in viscosity of molten slags with increasing mass ratio of BaO to CaO, which further attributes to the enhanced degree of polymerization of the aluminate network.

**KEYWORDS**

atomic pair distribution function, nuclear magnetic resonance, Raman spectroscopy, slags, structure, viscosity

## 1 | INTRODUCTION

Advanced high-strength steel (AHSS), including transformation-induced plasticity steel and twinning-induced plasticity steel have received intense interest in recent years because of their excellent combination of high strength, good ductility, and lower density.[1,2] In transportation applications, AHSS can be used to design structures with smaller material thicknesses, which saves weight and thereby decreases the fuel consumption and $CO_2$ emissions of vehicles.[3]

However, one of the challenging concerns for production of AHSS in industrial scale is the strong reaction between steel and mold fluxes during continuous casting,[4] which typically leads to problems of lubrication and heat transfer between mold and solidifying steel.[5] Mold fluxes play an indispensable role in continuous casting of steels and provide two critical functions as lubricating the steel shell and controlling the horizontal heat transfer. The fulfillment of functions for mold fluxes relies on the properties of mold fluxes, for example, viscosity at high temperature (more than 1000°C) and crystallization from molten and glassy fluxes. Therefore, one of the most important tasks for the production of AHSS is to develop mold fluxes that could meet the demand of smooth casting of steel. One solution for this is to develop nonreactive

This is an open access article under the terms of the Creative Commons Attribution License, which permits use, distribution and reproduction in any medium, provided the original work is properly cited.
© 2021 The Authors. *Journal of the American Ceramic Society* published by Wiley Periodicals LLC on behalf of American Ceramic Society (ACERS)

**TABLE 1** The chemical composition (weight percentage and molar percentage) of glassy samples investigated in the present study

| Sample No. | | CaO | $Al_2O_3$ | $B_2O_3$ | BaO | (CaO + BaO) | $T_g$ / °C |
|---|---|---|---|---|---|---|---|
| Ba0 | wt% | 49.1 ± 0.1 | 42.9 ± 0.1 | 8.0 ± 0.1 | 0 | 49.1 ± 0.1 | 762 ± 1 |
| | mol% | 62.1 ± 0.1 | 29.8 ± 0.1 | 8.1 ± 0.1 | 0 | 62.1 ± 0.1 | |
| Ba5 | wt% | 44.4 ± 0.1 | 43.4 ± 0.1 | 7.0 ± 0.1 | 5.2 ± 0.1 | 49.6 ± 0.1 | 764 ± 1 |
| | mol% | 58.6 ± 0.1 | 31.4 ± 0.1 | 7.4 ± 0.1 | 2.5 ± 0.1 | 61.1 ± 0.1 | |
| Ba10 | wt% | 39.1 ± 0.1 | 43.0 ± 0.1 | 7.7 ± 0.1 | 10.2 ± 0.1 | 49.3 ± 0.1 | 760 ± 1 |
| | mol-% | 53.7 ± 0.1 | 32.6 ± 0.1 | 8.5 ± 0.1 | 5.2 ± 0.1 | 58.9 ± 0.1 | |

or less-reactive mold fluxes for casting AHSS to restrict the reaction between mold fluxes and steels.[6] There are many types of nonreactive or less-reactive mold fluxes, for example, $CaO–Al_2O_3–B_2O_3$–based and $CaO–Al_2O_3–CaF_2$–based glass, have been developed in recent years[6–10]; however, their local interaction mechanism among individuals in structure has still been a great concern due to the effect of short-range structural ordering on properties.

BaO was reported to be one of the potential additives for optimization of physical properties of nonreactive or less-reactive mold fluxes. Xiao et al.[11] investigated the effect of BaO on the crystallization of $CaO–Al_2O_3$– based nonreactive mold fluxes and found that BaO shows a stronger tendency to inhibit crystallization of mold flux compared with $B_2O_3$. Yan et al.[9] found that the substitution of CaO with BaO retards the crystallization of $CaO–Al_2O_3$–based mold fluxes. Li et al.[12] measured the viscosity of $CaO–BaO–Al_2O_3–CaF_2–Li_2O$ mold fluxes with varied BaO substitution for CaO and found increased viscosity with increasing BaO as a substitute for CaO. Wang et al.[13] investigated the effect of substitution of CaO with BaO on the viscosity and structure of $CaO–BaO–SiO_2–MgO–Al_2O_3$ glass. These results showed that the viscosity of molten glass increased with increasing BaO substitution, which was correlated to an increase in the degree of polymerization of the glass.

$CaO–Al_2O_3–B_2O_3$–based mold fluxes have been proposed by many researchers as the most promising mold fluxes in casting of AHSS but still have some disadvantages, for example, strong crystallization and poor lubrication.[6,8] Because BaO was reported to inhibit the crystallization of mold fluxes, it will be very interesting to investigate the effect of BaO on the properties of $CaO–Al_2O_3–B_2O_3$-based mold fluxes. It has also been reported [13] that the physical properties of glass are strongly correlated to the structure, in particular the local structure due to the amorphous nature of glass. Therefore, understanding the effect of BaO on the local structure of $CaO–Al_2O_3–B_2O_3$-based mold fluxes is essential to the development of $CaO–Al_2O_3–B_2O_3$-based nonreactive mold fluxes. Only a few structural and viscosity studies on BaO-bearing mold fluxes were reported.[11–13] There is still a lack of insight on the effect of BaO on the local structure and its impact on the viscosity of $CaO–Al_2O_3–B_2O_3$ fluxes.

Aluminoborate glasses are interesting materials owing to their excellent dielectric, conductivity, chemical resistivity properties.[14–16] There have been many structural studies on aluminoborate glasses mainly using $^{27}Al$ and $^{11}B$ magic angle spinning nuclear magnetic resonance (MAS-NMR) and Raman spectroscopy.[23] However, these studies mainly focused on the glass compositions with network modifier content lower than 50 mol%. In comparison, mold fluxes usually have higher network modifier content to maintain a low viscosity value at high temperature.[6–9] It is necessary to investigate the structure and properties of aluminoborate systems with higher network modifier content to meet the demand for the development of mold fluxes.

In this work, the local structure of three $CaO–Al_2O_3–B_2O_3–BaO$ slags with varying mass ratio of CaO to BaO is determined by the total scattering atomic pair distribution function (PDF), Raman spectroscopy, and $^{27}Al$ and $^{11}B$ MAS-NMR. The total mass fraction of network modifier (CaO to BaO) is set to be 48%, and the molar fractions of network modifier (CaO and BaO) vary from 60.7% to 57.2% to simulate the practical composition of mold fluxes. The viscosity of $CaO–Al_2O_3–B_2O_3–BaO$ molten slags has been measured by the rotating cylinder method to support the structural characterization results.

## 2 | METHODS AND EXPERIMENT

### 2.1 | Sample preparation

Reagent grade $CaCO_3$, $BaCO_3$, $Al_2O_3$ and $H_3BO_3$ (all purity >99.5%) were adopted as raw materials. CaO was obtained by calcining $CaCO_3$ at 1050°C for 10 hours. $BaCO_3$ and $Al_2O_3$ powders was also calcined at 600°C to remove the moisture. The content of $B_2O_3$ in glasses were measured using inductively coupled plasma optical emission spectroscopy (Perkin Elmer, OPTIMA 7000DV) by dissolving glass in hydrochloric acid. The chemical compositions of glass samples are shown in Table 1.

The weighted powders were mixed and ground in an agate mortar, and then the powder mixtures were pressed into pellets. The pellets were put in a platinum crucible and melted

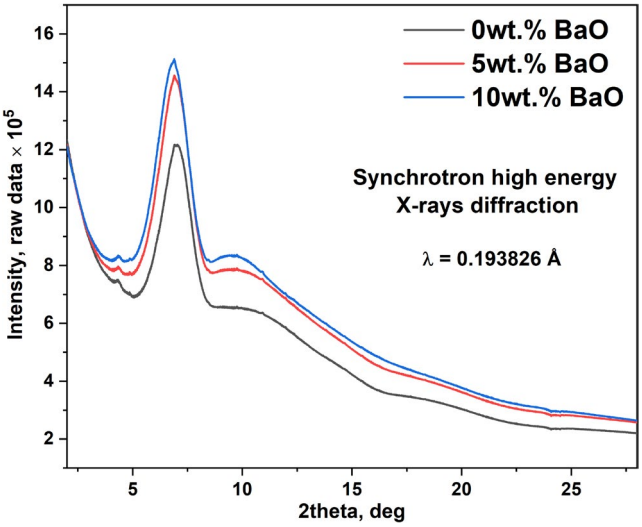


**FIGURE 1** Synchrotron X-ray diffraction patterns for all quenched samples [Color figure can be viewed at wileyonlinelibrary.com]

at 1550°C for 2 hours in a furnace with $MoSi_2$ as heating elements. After melting, the melts and crucible were taken out quickly from the furnace and quenched into the water. The amorphous states of quenched samples were verified by X-ray diffraction. Figure 1 shows high-energy synchrotron X-ray diffraction patterns for all the three samples, collected at the Canadian Light Source, indicating their short-range order. As seen in Figure 1, there are no crystalline peaks in all patterns, indicating the glassy state of all the studied samples. The high-energy diffraction data show a few peaks between 3 and 10°, indicating a very small amount of a crystalline phase, which is not the focus of this work. The glass transition temperatures of investigated glasses are determined by differential scanning calorimetry, which was performed using a thermal analyzer (Netzsch STA449F3) at a heating rate of 20°C/min. The measured glass transition temperatures are also listed in Table 1. Afterward, the quenched samples were subject to the Raman spectroscopy, MAS-NMR characterization and total scattering atomic PDF measurements.

## 2.2 | Raman spectral and MAS-NMR characterization

Raman spectroscopy measurements of these glassy samples were carried out on a laser confocal micro-Raman spectrometer (LabRAM HR evolution, Horiba). Raman spectra were acquired in the frequency range of 100 to 2000 $cm^{-1}$ by using He-Cd laser with an excitation wavelength of 532 nm. The acquired spectra were deconvolved by Gaussian peak function fittings.[24] The widths of peaks were set to be fixed during deconvolution procedures.

The $^{11}B$ and $^{27}Al$ MAS-NMR spectra were collected at a solid-state 600 MHz Fourier transform nuclear magnetic resonance spectrometer (Model: JNM-ECZ600R, Jeol ltd) at the field strength of 14.1 T(600 MHz), using a MAS probe with 3.2 mm $ZrO_2$ rotor. The resonance frequencies for $^{11}B$ and $^{27}Al$ are 192 MHz and 156 MHz. The Spinning rates were 18 kHz for $^{11}B$ and $^{27}Al$ MAS-NMR measurements. The relaxation delay time, pulse length, and tip angle are 5 s, 0.4 μs, and 18 degrees for $^{11}B$ and $^{27}Al$ MAS-NMR measurements, respectively. 1 M $AlCl_3$ and $H_3BO_3$ aqueous solutions were taken as reference materials for chemical shifts of $^{27}Al$ and $^{11}B$ spectra, respectively. The $^{11}B$ MAS-NMR spectra were fitted with the Dmfit program.[25,26] Second-order perturbation theory was used to simulate the peak of three-coordinated boron structural units, and Gaussian/Lorenz peak was used to simulate the contribution of four-coordinated boron.

## 2.3 | Viscosity measurements

The viscosities of molten slags were measured by a rotary-type viscometer (Brookfield, model DV2T). The spindle and crucibles for viscosity measurements were made by the molybdenum. The viscometer was calibrated at room temperature by using a standard silicone oil with a known viscosity value of 495 mPa·s. More detailed description of the viscometer can be found in our previous publication.[27]

Slags with a mass of 140 g were prepared and put in a molybdenum crucible, then the crucible was loaded in the even temperature zone of a vertical electrical resistance furnace with $MoSi_2$ rods as heating elements. High-purity argon (99.99%, 400 mL/min) was led into the furnace as a protective atmosphere. The slags were melted at 1873 K for 30 min and then cooled to the desired temperatures with a cooling rate of 5 K/min. After the furnace reached the desired temperature, the crucible was held at that temperature for 30 min to homogenize the melts. Then the working spindle (bob diameter: 14 mm; bob length: 20 mm; shaft diameter: 6 mm) was immersed in the middle of the molten glass, and the viscosities of the glass were measured at three different rotating speeds to confirm the Newtonian behavior of molten slag.

## 2.4 | High-energy diffraction and pair distribution function measurements

Total scattering data were collected on all three glass samples at the Brockhouse high-energy wiggler beamline of the Canadian Light Source using $\lambda = 0.193826$ Å radiation and a Perkin Elmer area detector with 200 × 200 μm pixels and a 40 × 40 cm area. The sample to detector distance was 154.3 mm. The wavelength was calibrated using a $LaB_6$ standard. The samples were loaded into Kapton capillaries

with 0.9 mm inner diameters. The data were processed using GSAS-II.[28] A $Q_{max}$ of 26 $Å^{-1}$ and Lorch dampening was used to produce the PDFs.

## 3 | RESULTS

### 3.1 | Theoretical consideration

Extensive spectroscopic studies have been performed on the structure of alkali metal or alkali earth metal aluminoborate. Although the compositions of these glasses have lower content of network-modifying oxide than the present glasses. The structural knowledge of aluminoborate glasses derived by these studies can be extrapolated to give the hints for the structures of the present glasses.

According to the previous NMR studies, the charge compensation of $AlO_4^{5-}$ by alkali metal cations or alkali earth metal cations is preferable compared with the formation of BO4. Besides, according to the glass composition listed in Table 1, the present glasses have larger amounts of alkali earth metal cations than the previously investigated glasses. The amount of $Ca^{2+}$ and $Ba^{2+}$ is much more than that required for the charge compensation. Therefore, it is speculated that the aluminums in the present glasses mainly exist in four-coordination. However, the possible existence of minor five-coordinated aluminum ($Al^{V}$) and six-coordinated aluminum ($Al^{VI}$) should be checked by $^{27}$Al MAS-NMR.

In borate and borosilicate glasses,[47–49] the initial addition of network modifiers leads to the conversion of three-coordinated boron ($B^{III}$) to four-coordinated boron ($B^{IV}$) with little or no formation of nonbridging oxygen (NBO). The four-coordinated boron can further convert to three-coordinated boron groups with 1, 2, and 3 NBOs if enough network modifiers are added. In sodium aluminoborate glasses, three-coordinated boron species containing 1 or 2 NBO has been found in glass composition with relatively high concentration of network-modifying oxide by $^{11}$B MAS-NMR.[18] The present glasses have even higher content of network-modifying oxide than glasses in literature.[18] Therefore, it is presumed that most of the four-coordinated boron has been converted into three-coordinated boron groups. The three-coordinated boron groups should dominate the structure of borate. Fully depolymerized three-coordinated boron species (with three NBOs) could be found in glass structure. The abundance of $B^{III}$ and $B^{IV}$ can be easily obtained from the $^{11}$B MAS-NMR performed at high field strength, and the presumption of dominance of $B^{III}$ can be verified.

Apart from the role of charge compensator, alkali earth metal cations can also lead to the formation of NBO associated with $Al^{IV}$, $B^{III}$, $B^{IV}$. According to the above analyses, the $B^{IV}$ should be minor due to the large amount of network-modifying oxide in the present glasses. Therefore, there is a competition between $B^{III}$ and $Al^{IV}$ for the formation of NBO. It was proposed that the formation of NBO associated with Al is energetically less stable than NBO associated with B due to its higher localized charge (formal charges of B/NBO and Al/NBO are −1.0 and −1.25, respectively). If we assume that NBO is preferentially connected with boron, we can calculate the NBO numbers associated with $B^{III}$ per boron site (NBO/B) from glass composition. For all samples, the NBO/B values can be calculated as 3, indicating that all boron exists as orthoborate. The NBO number associated with Al per aluminum site (NBO/Al) can be further calculated because extra network-modifying cation will depolymerize the aluminate network. The calculated NBO/Al values are 0.27, 0.24, and 0.02. However, this calculation assumes complete B-NBO preference. The contribution of less depolymerized boron group (e.g., $B^{III}$ with one bridging oxygen) could be probably found in NMR and Raman spectra, and the NBO/Al values based on spectroscopic data could be larger.

### 3.2 | Structural characterizations

To characterize the short-range ordering of these glasses, $^{11}$B and $^{27}$Al MAS-NMR were performed on these glass samples. The $^{11}$B MAS-NMR spectra are shown in Figure 2. As can be seen in the figure, there is a broad envelope ranging from 5 to 22 ppm accompanied with a slight peak centered around 2 ppm. The strong broad envelope ranging from 5 to 22 ppm can be attributed to the resonance shift of three-coordinated boron ($B^{III}$).[29–31] Based on previous NMR studies,[29–31] the minor peak centered at around 2 ppm can be assigned to four-coordinated boron ($B^{IV}$). It can be seen from Figure 2 that three-coordinated boron $B^{III}$ dominates boron species with

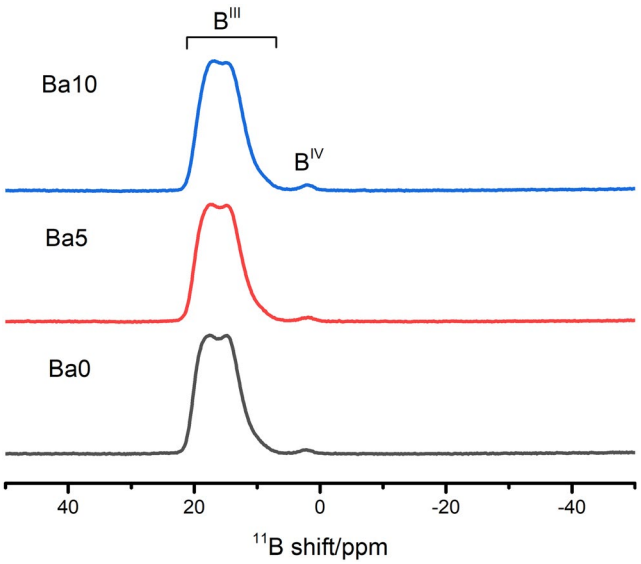


FIGURE 2 $^{11}$B MAS-NMR spectra for various samples [Color figure can be viewed at wileyonlinelibrary.com]

the presence of some minor $B^{IV}$, which is consistent with the analysis based on previous studies on boroaluminate glass. After subtracting the baseline, the peaks for $B^{III}$ and $B^{IV}$ are integrated to calculate the areas of peaks from which the molar percentages of $B^{III}$ and $B^{IV}$ can be readily obtained. The calculated molar percentages of $B^{IV}$ are 1.46 ± 0.01%, 1.18 ± 0.01%, and 1.36 ± 0.01% for Ba0, Ba5, and Ba10, respectively, indicating that there is only a minor existence of $B^{IV}$ in the present glasses.

The $^{11}B$ MAS-NMR spectra can be further fitted by using the Dmfit program, and fitting results are shown in Figure 3. The sharp peak near 2 ppm can be simulated by using the Gaussian function indicating that quadrupole coupling is weak due to the local symmetry of $B^{IV}$. The broad envelope ranging from 5 to 22 ppm due to three-coordinated boron sites reflects the strong second-order quadrupolar effects and can be deconvolved by assuming second-order perturbation theory implemented in Dmfit. It should be mentioned that all quadrupolar coupling parameters should be in distributions for glasses. For simplicity, here, only singular parameters were used for fitting to reproduce the experimentally observed line shape of glasses. It was found that a single peak cannot represent the broad peak of $B^{III}$, indicating multispecies borate in structures of glasses. For the sake of simplification, two peaks with isotropic chemical shift ($\delta_{iso}$) near 21 ppm and 19.5 ppm were used to simulate the broad envelope ranging from 5 to 22 ppm. According to NMR research on crystalline boron compound by Kroeker and Stebbins,[32] the peak with $\delta_{iso}$ at around 21 ppm can be attributed to the orthoborate ($T^0$, $T^n$ indicates trigonal boron with n bridging oxygen) with zero bridging oxygen. This is consistent to our analysis in the section of theoretical consideration that orthoborate should be preferable in structures of all glasses. The peak at lower $\delta_{iso}$ (19.5 ppm) can be attributed to the contribution of the boron connected ($T^1$) with single bridging oxygen,[18] which could be pyroborate or $B^{III}$–O–$Al^{IV}$.

The deconvolution results for $^{11}B$ MAS-NMR spectra are shown in Figure 3. The fitting parameters including calculated area fraction ($N_{T0}$, $N_{T1}$, and $N_4$ for $T^0$, $T^1$, and $B^{IV}$, respectively), $\delta_{iso}$, and quadrupole coupling parameters ($P_Q$) are summarized in the Table 2. It can be seen from Table 2 that the orthoborate structural unit is the main borate group in glass structures. There are also some $T^1$ groups accounting for 14%–29% of structural groups. The existence of some $T^1$ groups indicates the incomplete preference of B-NBO. As BaO content increases, the area fractions of $T^1$ groups gradually increase. Only minor four-coordinated boron (1%–2%) can be found in glass structure.

Figure 4 shows the $^{27}Al$ MAS-NMR spectra for all studied samples. It can be seen from the figure that there is a strong peak centered at around 78 ppm, which reflects tetrahedral coordinated aluminum ($Al^{IV}$).[17–23,33,34] It can be further observed that the peak is asymmetric and there are tails between 40 and 70 ppm, reflecting well-known second-order

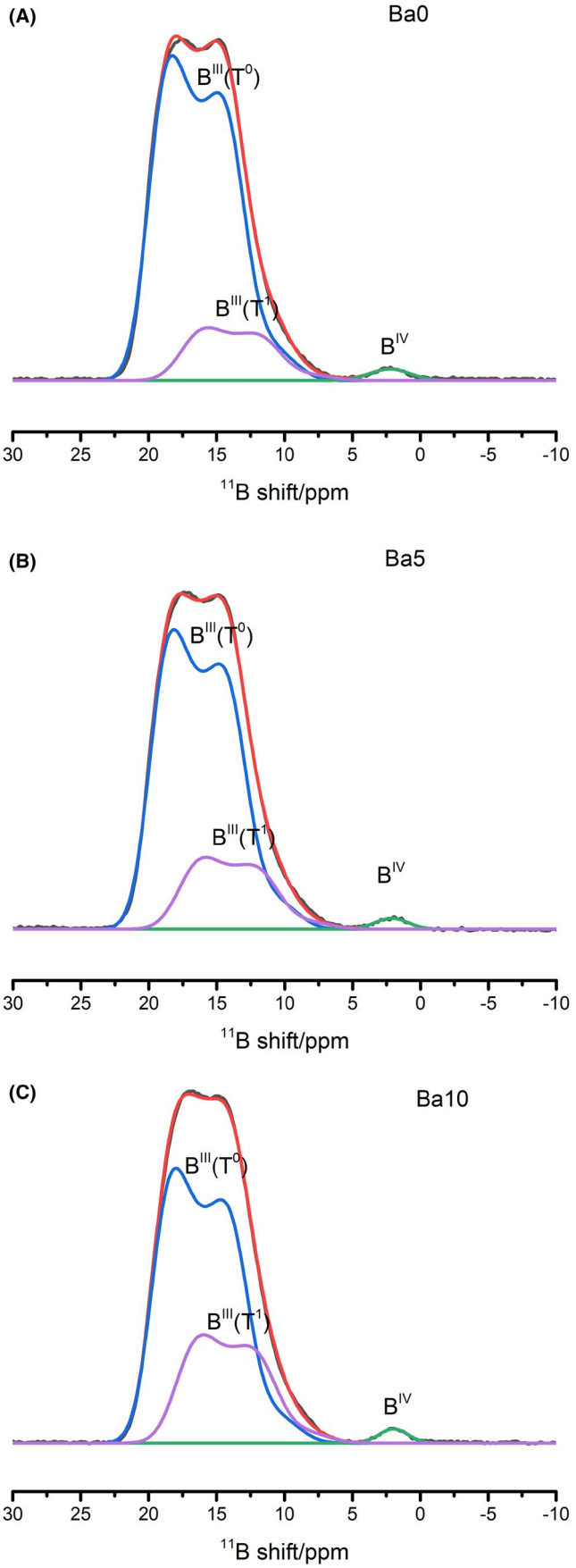


**FIGURE 3** Experimental and simulated $^{11}B$ MAS-NMR spectra of various samples (A) Ba0; (B) Ba5; and (C) Ba10 [Color figure can be viewed at wileyonlinelibrary.com]

**TABLE 2** $^{11}$B NMR fitting parameters of the glasses investigated in the present work

| | $T^0$ | | | $T^1$ | | | $B^{IV}$ | |
|---|---|---|---|---|---|---|---|---|
| **Sample No.** | $N_{T0}$ / % | $\delta_{iso}$ / ppm | $P_Q$ / KHz | $N_{T1}$ / % | $\delta_{iso}$ / ppm | $P_Q$ / KHz | N4 / % | $\delta_{iso}$ / ppm |
| Ba0 | 84.2 ± 0.1 | 21.1 ± 0.1 | 2662 ± 5 | 14.4 ± 0.1 | 18.7 ± 0.1 | 2713 ± 5 | 1.5 ± 0.1 | 2.2 ± 0.1 |
| Ba5 | 79.0 ± 0.1 | 21.0 ± 0.1 | 2662 ± 5 | 19.8 ± 0.1 | 18.9 ± 0.1 | 2713 ± 5 | 1.2 ± 0.1 | 2.1 ± 0.1 |
| Ba10 | 69.8 ± 0.1 | 20.8 ± 0.1 | 2662 ± 5 | 28.9 ± 0.1 | 19.1 ± 0.1 | 2713 ± 5 | 1.3 ± 0.1 | 2.0 ± 0.1 |

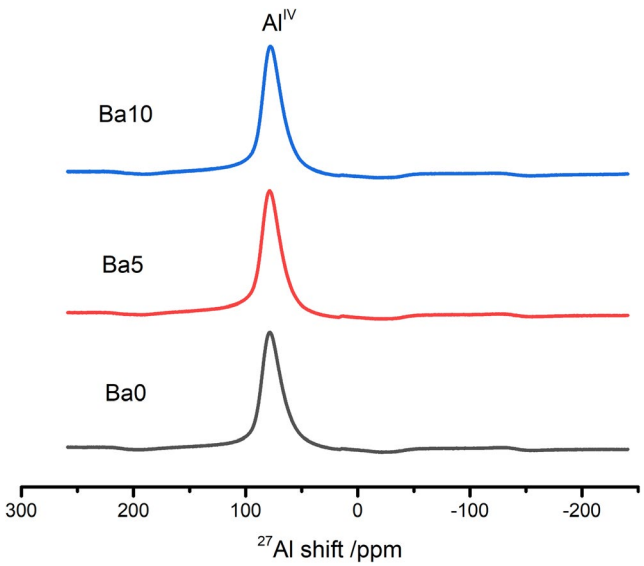


**FIGURE 4** $^{27}$Al MAS-NMR spectra of various samples [Color figure can be viewed at wileyonlinelibrary.com]

quadrupolar effects found in NMR spectra for nucleus with the spin quantum number greater than ½ (e.g., $^{27}$Al and $^{11}$B).[35,36] No signals of five-coordinated aluminum $Al^V$ (located at around 30 ppm) and six-coordinate aluminum ($Al^{VI}$) (located at around 10 ppm)[17–23] were found in spectra for all samples. It can be concluded that aluminum exclusively exists as four-coordinated Al in the present glasses.

Raman spectroscopy was used to further investigate the short-ranged order and medium-ranged order in glasses. Figure 5 shows the Raman spectra of glassy samples investigated in the present work. The experimentally observed Raman spectra are similar to the previous Raman investigation results on $CaO–Al_2O_3–B_2O_3$,[23,37] $CaO–Al_2O_3–B_2O_3–Na_2O$,[38] and $CaO–Al_2O_3–B_2O_3–Li_2O–Na_2O$ [39] systems. The strong Raman bands around 550 cm$^{-1}$ should be attributed to the transverse motion of bridging oxygen within $Al^{IV}$–O–$Al^{IV}$ linkages.[34,40,41] A small shoulder of 550 cm$^{-1}$ band can be found at around 630 cm$^{-1}$, which can be attributed to the transverse motion of bridging oxygen within $Al^{IV}$–O–$B^{III}$ linkages.[38,39] It can be speculated that parts of $T^1$ species in NMR spectra exist in the form of $Al^{IV}$–O–$B^{III}$ linkages. The bands at around 780 cm$^{-1}$ (should be the envelope of various bands due to large full width at half maximum) mainly reflect the Al–O stretch vibrations of $AlO_4$ tetrahedral structural units with different numbers of NBO.[23,34,40–42] As shown in Figure 5, the intensity of bands centered around 780 cm$^{-1}$ obviously decreases with increasing BaO content in the glass. The area ratio of higher-frequency band at 780 cm$^{-1}$ to low-frequency band at 550 cm$^{-1}$ decreases as BaO content in the glass increases. Licheron et al.[34] investigated the structure of calcium-, strontium- and barium-aluminate glasses using Raman spectroscopy. They also observed the area ratio of higher-frequency band at 780 cm$^{-1}$ to low-frequency band at 550 cm$^{-1}$ decreases as the glass composition changes from $Ca_3Al_2O_6$ to $CaAl_2O_4$. The $(CaO + BaO)/Al_2O_3$ ratios for the present glasses are between 1.6 and 2.1. According to calculated NBO/Al values from the B-NBO preference model, the aluminum tetrahedron should be essentially in $Q^3$(Al) and $Q^4$(Al), where $Q^n$(Al) indicates aluminum in tetrahedral sites with n bridging oxygen. Bands centered around 780 cm$^{-1}$ include the contributions from both $Q^3$(Al) and $Q^4$(Al),[23,34] whereas the low-frequency Raman bands around 550 cm$^{-1}$ only reflect transverse motion of bridging oxygen within Al-O-Al linkages. Therefore, the decrease in the area ratio of higher-frequency band at 780 cm$^{-1}$ to low-frequency band at 550 cm$^{-1}$ reflects the possible decrease of NBOs. The strong bond at around 920 cm$^{-1}$ is frequently observed in some glassy aluminoborate slag with high concentration of network-modifying oxides.[37,39] According to Raman study on borate glasses, this band can be assigned to be the vibration of orthoborate ($BO_3$) structural units.[43–45] This is in line with the NMR results on that the dominant structural group for borate in structure of the present glasses is orthoborate. The lack of bands at higher frequency range in the present spectra indicates that there are no B-O$^-$ bonds attached to large borate groups in present glasses.[46] This is also consistent with the NMR results which indicate only presences of small borate groups.

The bands within 400–1100 cm$^{-1}$ can be deconvolved by assuming Gaussian peaks for various structural units to further separate the overlapping contributions of various structural units. The deconvolution parameters including the frequencies of peaks, areas are summarized in Table 3. The deconvolution results for Raman spectra are shown in Figure 6. Two vibration peaks of $Al^{IV}$–O–$Al^{IV}$ (at around 550 cm$^{-1}$)[21–24] and $Al^{IV}$–O–$B^{III}$[19,20] (~630 cm$^{-1}$) were used to represent the bands between 450 and 670 cm$^{-1}$.

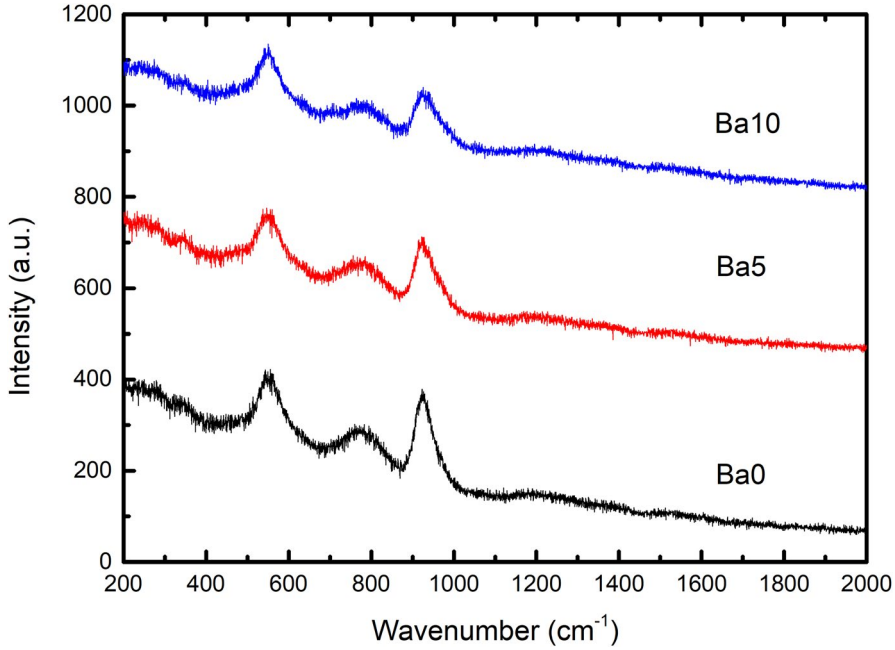


**FIGURE 5** The Raman spectra of glass samples with varying BaO content [Color figure can be viewed at wileyonlinelibrary.com]

The bands within 700–800 $cm^{-1}$ are deconvolved by considering peaks contributed to two $AlO_4$ structural units: $Q^3$(Al) (at around 740 $cm^{-1}$) and $Q^4$(Al) (at around 790 $cm^{-1}$).[18,21–25] NMR simulation on $^{11}$B MAS-NMR spectra indicates the possible existence of $T^1$ group, which reflects pyroborate or linkage of $Al^{IV}$–O–$B^{III}$. The vibration of $Al^{IV}$–O–$B^{III}$ has been reflected by the shoulder (630 $cm^{-1}$) of $Al^{IV}$–O–$Al^{IV}$. According to the previous Raman study on borate,[43–45] the band at 820 $cm^{-1}$ reflects the vibration of the pyroborate group and can be included in the present Raman deconvolution. The band at 930 $cm^{-1}$ can be successfully deconvolved using a single Gaussian peak attributed to the vibration of the orthoborate group.

The PDF, G($r$), shows the distributions of all atom–atom distances in a sample and can provide information on the local structure of an amorphous material. The PDFs of the three glass samples are plotted together in Figure 7. The most intense feature in all three PDFs is a sharp peak at 1.76 Å, which can be assigned to the Al–O bond distance. Bond valence considerations indicate that the average bond length for Al with coordination numbers of 4, 5, and 6 should be 1.76, 1.84, and 1.91 Å, respectively. The perfect match with the expected value for tetrahedral Al and the lack of any shoulders on these peaks confirm that essentially all Al is tetrahedral in all samples. This result is in agreement with the Raman and NMR results, which show predominantly tetrahedral Al. The very small amount of octahedral Al seen by NMR is likely too small to be observed by PDF. Although the maximum intensity of the Al–O peak decreases with increasing Ba content this does not seem to be due to any significant change in the coordination number. A small part of this decrease can be attributed to the lower density of Al–O bonds as the larger Ba is introduced, but mostly to an increase in the widths of the peaks. By converting G($r$) to the radial distribution function, R($r$), and integrating the area underneath the peak it is possible to obtain the coordination number of Al. This procedure yielded values of 4.06, 3.93, and 4.14 for samples with 0%, 5%, and 10% Ba, respectively, all quite close to the expected value of 4 for tetrahedral coordination. The increase in peak widths indicates a broader distribution of Al–O bond lengths, suggesting the tetrahedra become less regular as the Ba content increases. This trend can be linked to the increase in polymerization. An $AlO_4$ with several terminal O atoms can easily form a nearly ideal tetrahedron, but as it becomes connected to more other polyhedra the tetrahedron will need to distort in order to connect to them all.

A weak peak is observed between ~1.3 and 1.4 Å which can be ascribed to B–O bond lengths. For the Ba free sample, the peak is at 1.35 Å, whereas for the samples containing Ba these peaks increase in intensity and shift to 1.38 and 1.37 Å. Some caution is needed when interpreting this peak due to the low contribution of B–O bonds to the PDF, potential overlap with low-$r$ termination noise, and overlap with the tail of the much stronger Al–O peak. However, an increase in distance and intensity is consistent with an increase in the number of $T^1$ groups relative to the number of orthoborates as revealed by the NMR data.

The next peak at ~2.36 Å can be attributed primarily to Ca–O bond lengths, although nearest neighbor B–Al and B–B distances may also contribute to a much smaller extent. The intensity of this peak decreases rapidly as the Ba concentration increases, which is not surprising as the Ca concentration is decreasing. It appears that some decrease is also due to a broadening of the peak, suggesting less regular coordination for Ca with increasing Ba. In the two samples containing Ba, there is a weak, broad feature at ~2.65 Å which is absent in the Ba free sample and can be assigned to Ba–O

**TABLE 3** Peak frequencies ($\upsilon$/cm$^{-1}$) and peak area ($A$) of Raman bands obtained from deconvolution for various samples

| Sample No. | Al–O–Al | | Al–O–B | | $Q^3$(Al) | | $Q^4$(Al) | | Pyroborate | | Orthoborate | |
|---|---|---|---|---|---|---|---|---|---|---|---|---|
| | $\nu$ | $A$ | $\nu$ | $A$ | $\nu$ | $A$ | $\nu$ | $A$ | $\nu$ | $A$ | $\nu$ | $A$ |
| Ba0 | 552 ± 1 | 9268 ± 5 | 621 ± 1 | 2285 ± 5 | 746 ± 1 | 3611 ± 5 | 797 ± 1 | 3315 ± 5 | 820 ± 1 | 985 ± 5 | 928 ± 1 | 10955 ± 5 |
| Ba5 | 548 ± 1 | 6723 ± 5 | 606 ± 1 | 1629 ± 5 | 742 ± 1 | 2219 ± 5 | 787 ± 1 | 2562 ± 5 | 824 ± 1 | 1349 ± 5 | 930 ± 1 | 7362 ± 5 |
| Ba10 | 547 ± 1 | 7815 ± 5 | 620 ± 1 | 1444 ± 5 | 736 ± 1 | 1178 ± 5 | 783 ± 1 | 1965 ± 5 | 814 ± 1 | 604 ± 5 | 934 ± 1 | 6010 ± 5 |

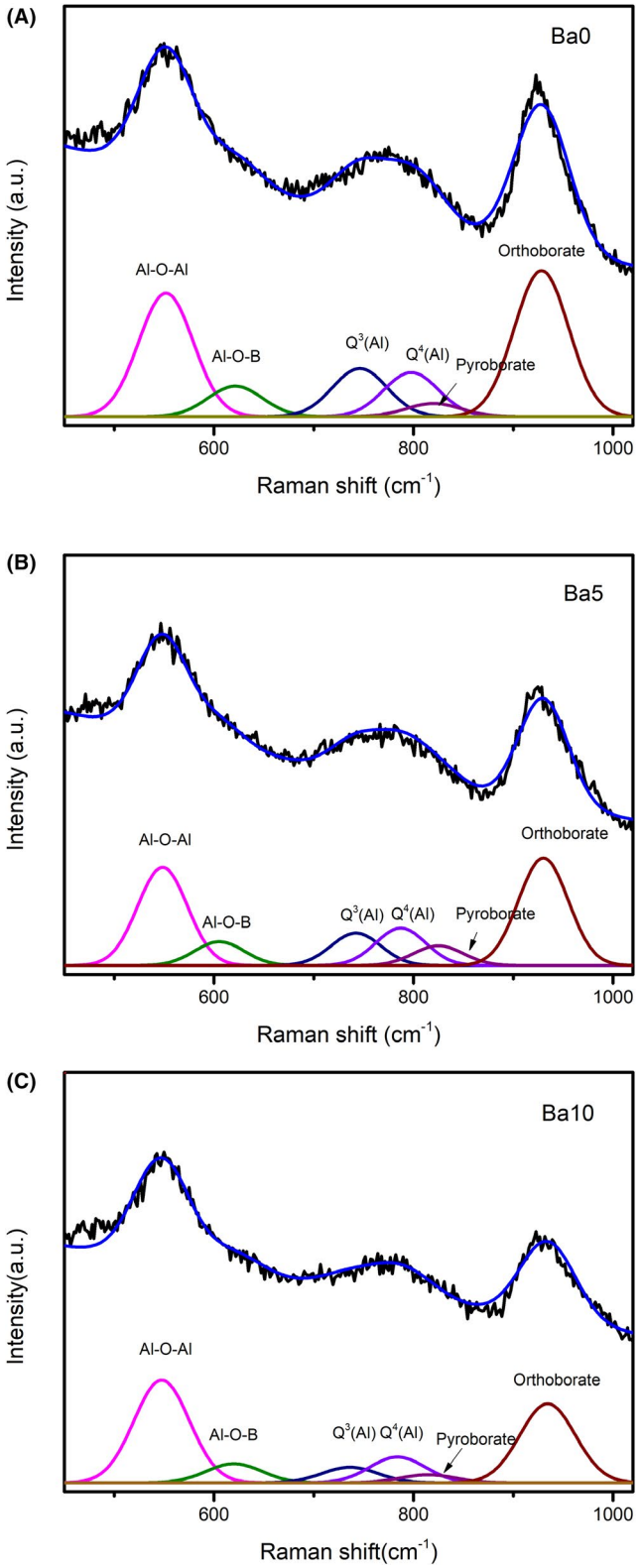


**FIGURE 6** Deconvolution results of Raman spectra (A) Ba0; (B) Ba5; and (C) Ba10 [Color figure can be viewed at wileyonlinelibrary.com]

bond lengths. These bonds make a noticeable contribution to the PDF despite the low Ba concentration because Ba is a

much stronger X-ray scatter compared with any of the other elements present.

Nearest neighbor O–O distances are expected around 2.9 Å and can explain the rise in the PDF in this region. The broad feature around ~3.2–3.3 Å is primarily due to nearest neighbor Al–Al distances, with second nearest neighbor B–O also making a much smaller contribution in this region. The broadness of these features shows that the Al–O–Al angle varies somewhat, which is consistent with the amorphous nature of these materials. The last strong feature around ~3.6 Å is primarily due to second nearest neighbor Al–O distances. Beyond ~3.8 Å the PDF has contributions from all types of atom–atom pairs. Broad features can be seen up until roughly 16 Å, beyond which the PDF becomes flat indicating a complete lack of structural correlation past this distance. The correlation length does not seem to vary significantly with composition.

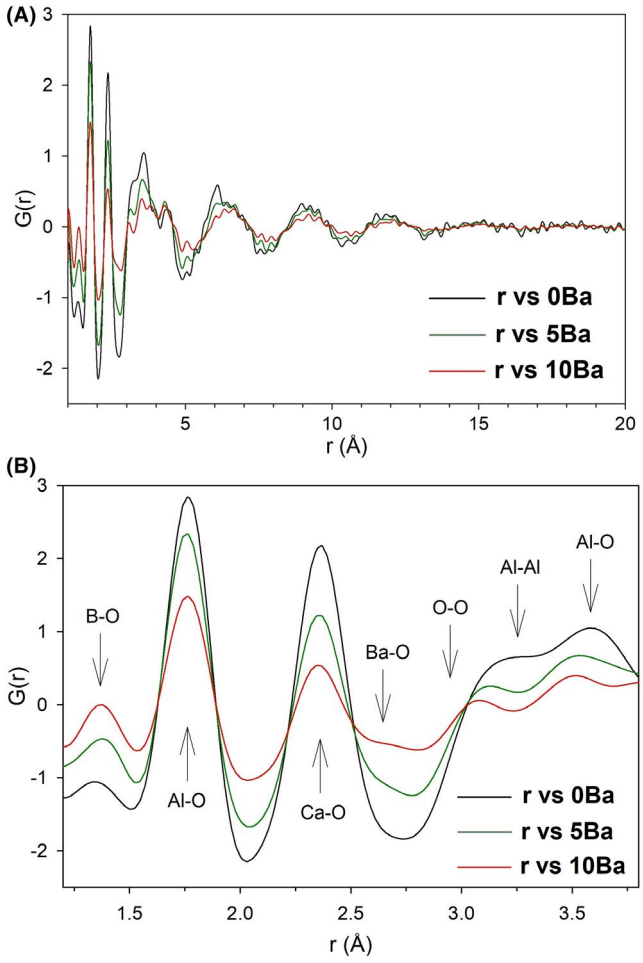


**FIGURE 7** Total scattering pair distribution function data for all the samples showing possible distributions of all atom–atom distances. A) in an extended region and B) enlarged part [Color figure can be viewed at wileyonlinelibrary.com]

## 3.3 | Viscosity measurements

The viscosities of molten slags in the temperature range from 1460°C to 1600°C were measured by the rotating spindle method. Measured viscosity values for various samples are shown in Table 4. As seen from the table, the viscosity of slags increases with increasing BaO content in slags at the same temperature, and the viscosity of slag decreases with increasing temperature.

It is well accepted that the temperature dependence of the viscosity of molten slag can be well described by the Arrhenius-type equation:

$$\eta = A\exp\left(\frac{E}{RT}\right) \tag{1}$$

where $A$ is the pre-exponential factor, $E$ is viscous activation energy, $R$ is gas constant, and $T$ is temperature in K.

The Equation (1) could be transformed into the following equation:

$$\ln\eta = \ln A + \frac{E}{RT} \tag{2}$$

The present experimental data can be fitted by plotting $\ln\eta$ versus $1/T$ shown in Figure 8. It can be seen from this figure that plots of $\ln\eta$ versus $1/T$ follow a linear relationship for all samples. There is no inflection point found in $\ln\eta$ versus $1/T$ plot. This also indicates that all slag samples are in a liquid state in the temperature range of 1733–1873 K and there was no crystal precipitation during viscosity measurements.

The viscous activation energy reflects the energy barrier for viscous flow of molten slag. Viscous activation energy for all samples may be calculated from the slope of the fitting lines. Calculated viscous activation energies of various samples are also shown in Table 6. It can be seen that the viscous activation energies also increase as BaO content in slag increases.

**TABLE 4** Measured viscosity values and calculated viscous activation energies $E_\eta$ for samples investigated in the present work

| | Viscosity values (mPa.s) at various temperatures (°C) | | | | | | |
|---|---|---|---|---|---|---|---|
| Sample no | 1600 | 1560 | 1540 | 1500 | 1480 | 1460 | $E_\eta$ (kJ/mol) |
| Ba0 | 103.98 ± 0.69 | 125.63 ± 1.433 | 141.35 ± 0.949 | 181.19 ± 0.799 | 194.47 ± 1.19 | 227.01 ± 0.45 | 150.08 ± 4.4 |
| Ba5 | 108.11 ± 0.14 | 131.65 ± 0.39 | 147.66 ± 0.48 | 183.84 ± 1.54 | 210.93 ± 0.64 | 248.62 ± 1.86 | 158.33 ± 5.2 |
| Ba10 | 119.44 ± 0.23 | 146.75 ± 0.73 | 161.64 ± 1.28 | 208.97 ± 0.84 | 240.14 ± 0.25 | 280.27 ± 1.02 | 164.27 ± 4.9 |

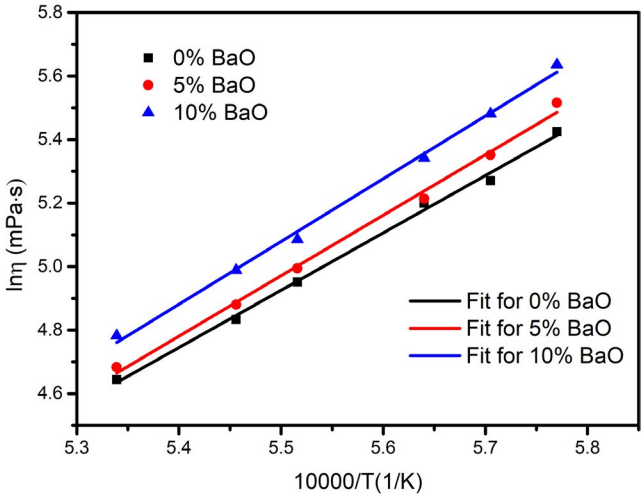


**FIGURE 8** Values of logarithm of viscosity as functions of the reciprocal of temperature for slags [Color figure can be viewed at wileyonlinelibrary.com]

## 4 | DISCUSSION

From the present MAS-NMR, Raman spectroscopy, and PDF study, the aluminums in the present glasses are found to be exclusively tetrahedral coordinated aluminums. Because a large amount of CaO and BaO exist in the present glass ((CaO + BaO)/$Al_2O_3$ > 1), a full-charge compensation of tetrahedral coordinated aluminum can be assumed and there should be negligible five- or six-coordinated aluminum. This is in line with the previous investigation on aluminoborate glasses with M/$\nu$Al > 1 ($\nu$ is the valence of M).[22] Apart from charge compensation, CaO and BaO in the present glasses can play another role as network-modifying oxide. The excess CaO and BaO will depolymerize the network built by tetrahedral aluminate.[34] The present glasses also some boron species, which could compete for de-polymerization by network-modifying oxides. Therefore, the degree of depolymerization for aluminate networks will be discussed together with the existence of borate species.

According to the present $^{11}$B MAS-NMR, Raman spectroscopy, and PDF study, the dominant boron group in the present glasses is orthoborate ($BO_3^{3-}$), a trigonal borate structure with three NBOs. There are some existences of $T^1$ group, which is the trigonal borate structure with two NBOs. The present glasses have even higher content of network-modifying oxide than glasses in literature.[18] Therefore, most four-coordinated boron has converted into a three-coordinated boron group with three NBOs. Some $B^{IV}$ converts into three-coordinated boron groups with two NBOs. This indicates that boron species are predominantly depolymerized into isolated orthoborate groups with three NBOs and borate groups with two NBOs. Some $B^{III}$ with two NBOs will form the pyroborate group. It is also probable that some $B^{III}$ with two NBOs will connect with $Al^{IV}$ to form $Al^{IV}$–O–$B^{III}$, which is favorable according to previous studies.[18–22] The existence of pyroborate group and $Al^{IV}$–O–$B^{III}$ has been detected by Raman spectroscopy.

The speciation of boron and aluminum sites afforded by NMR, Raman spectroscopy and PDF provides opportunities to estimate the network connectivity in the glass structure. For the present depolymerized glasses, the degree of polymerization is essential for understanding variation of properties from a structural point of view. According the fitting on $^{11}$B spectra, the NBO/B values for 0Ba, 5Ba, and 10Ba glasses are 2.86, 2.80, and 2.71, respectively. The calculated NBO/Al values based on the boron speciation for 0Ba, 5Ba, and 10Ba glasses are 0.32, 0.29, and 0.11 respectively, which are higher than the values calculated from complete B-NBO preference. According to NBO/Al values both from NMR fitting and complete B-NBO preference model, the NBO/Al decreases as mass percentage of BaO increases, which can be attributed to the amount decrease of network-modifying oxides (CaO + BaO). Accordingly, the connectivity and the degree of polymerization of aluminate network in structure of the present glasses increases with increasing mass percentages of BaO.

As given in Table 1, the glass transition temperature first increases and then decreases with increase of BaO content. The glass transition temperatures in the present glasses can be both affected by network connectivity and field strength of network-modifying cations. The first increase in the glass temperature should be attributed to the enhanced network connectivity due to the decreasing amount of network-modifying oxides. The following drop of glass transition temperatures is related to the introduction of $Ba^{2+}$ (ionic radius: 1.61 Å[50]) with weaker field strength than $Ca^{2+}$ (ionic radius:1.01 Å[50]), which leads to the weaker glass network and a lower glass transition temperature. This effect of cation field strength has been investigated[51] by substituting $Ca^{2+}$ with low-field-strength cations ($Sr^{2+}$ and $Ba^{2+}$) in calcium aluminate.

The viscous activation energy can be associated with the local structure of molten slag.[52,53] According to present NMR, PDF, and Raman studies, the structure of glasses comprises of aluminate network and some ortho and pyroborate groups. The isolated orthoborate and T1 groups have simple forms, which are easy for viscous shearing. The main obstacle for viscous flow is the aluminate network in present glasses. The structural characterizations have shown that the degree of polymerization of aluminate networks in glassy glass is enhanced as BaO content increases. The enhanced polymerization of aluminate networks indicates that the network and the flow structural units are more complex. More bonds in slag with a more complex structure would be broken by shearing, leading to increased energy barrier for viscous flow.

The field strength of network-modifying cation should also have some effects on the viscosity of slags. The $Ba^{2+}$ has a weaker field strength (defined by $z/r^2$, z is the valence number of metal ions, and r is the radius of cations) than $Ca^{2+}$.

The bond strength of Ba-O-Al should be weaker than Ca-O-Al and easier to be broken during viscous shearing. Thus, the viscous flow is facilitated and a lower viscosity can be expected by introduction of $Ba^{2+}$. However, the viscosity of the present slag increases with increasing BaO content, indicating that the field strengths of network-modifying cations are not critical to viscous flow. The viscous flows in the present glasses are mainly influenced by the degree of polymerization in the aluminate network.

## 5 | CONCLUSIONS

By using the atomic PDF, Raman spectroscopy, $^{27}Al$ and $^{11}B$ MAS-NMR, the structure of $CaO–Al_2O_3–B_2O_3–BaO$ slag with varying mass ratio of BaO to CaO was uncovered. The viscosity of $CaO–Al_2O_3–B_2O_3–BaO$ slag was determined by rotating cylinder method to investigate the correlation between the structure and properties of glasses. The following conclusions can be drawn from this work:

1. $^{11}B$ MAS-NMR data showed that boron in glass is mainly three-coordinated. The simulation on NMR spectra further indicates that the dominant boron group is orthoborate with zero bridging oxygen. Some (14%–29%) three-coordinated boron species with one bridging oxygen and minor (less than 2%) four-coordinated boron species can be also resolved by simulation.
2. $^{27}Al$ MAS-NMR showed that aluminums in the present glasses are exclusively in tetrahedral coordination.
3. Raman spectral study showed that the transverse vibration of $Al^{IV}–O–Al^{IV}$ and $Al^{IV}–O–B^{III}$, stretching vibration of aluminate structural units and vibration of orthoborate and pyroborate structural groups.
4. The PDF results showed tetrahedral coordination for all Al, whereas a broader distribution of Al–O bond lengths indicates less regular tetrahedra with increasing Ba. An increase in distance and intensity of the B–O peak is consistent with a slight increase in the number of pyroborate and tetrahedral B relative to the number of orthoborate.
5. With increase of BaO content, the viscosity and viscous activation energy of slags increases. The increased viscous activation energy reflects the enhanced degree of polymerization in glass structure.

## ACKNOWLEDGMENTS

Authors acknowledge the financial support from Academy of Finland grant #311934. We also thank the Center of Microscopy and Nanotechnology, University of Oulu. The authors also acknowledge the financial support from National Natural Science Foundation of China (NSFC No. 51774026). Part of the research described in this paper was performed at the Canadian Light Source, a national research facility of the University of Saskatchewan, which is supported by the Canada Foundation for Innovation (CFI), the Natural Sciences and Engineering Research Council (NSERC), the National Research Council (NRC), the Canadian Institutes of Health Research (CIHR), the Government of Saskatchewan, and the University of Saskatchewan.

## ORCID

*Qifeng Shu* https://orcid.org/0000-0001-5434-3314

## REFERENCES

1. Soleimani M, Kalhor A, Mirzadeh H. Transformation-induced plasticity (TRIP) in advanced steels: a review. Mater Sci Eng, A. 2020;795:140023.
2. De Cooman BC, Estrin Y, Kim SK. Twinning-induced plasticity (TWIP) steels. Acta Mater. 2018;142:283–362.
3. Grajcar A, Kuziak R, Zalecki W. Third generation of AHSS with increased fraction of retained austenite for the automotive industry. Archives Civil Mech Eng. 2012;12:334–41.
4. Kim MS, Lee SW, Cho JW, Park MS, Lee HG, Kang YB. A reaction between high Mn-high Al steel and CaO-SiO 2-type molten mold flux: part I. Composition evolution in molten mold flux. Metall Mater Trans B. 2013;44(2):299–308.
5. Street S, James K, Minor N, Roelant A, Tremp J. Production of high-aluminum steel slabs. Iron Steel Technol. 2008;5(7):38–49.
6. Cho JW, Blazek K, Frazee M, Yin H, Park JH, Moon SW. Assessment of $CaO–Al_2O_3$ based mold flux system for high aluminum TRIP casting. ISIJ Int. 2013;53(1):62–70.
7. Liu Q, Wen G, Li J, Fu X, Tang P, Li W. Development of mold fluxes based on lime–alumina slag system for casting high aluminum TRIP steel. Ironmaking Steelmaking. 2014;41(4):292–7.
8. Li J, Kong B, Galdino B, Xu J, Chou K, Liu Q, et al. Investigation on properties of fluorine-free mold fluxes based on $CaO–Al_2O_3–B_2O_3$ system. Steel Res Int. 2017;88(9):1600485.
9. Yan W, Chen W, Yang Y, Lippold C, Mclean A. Effect of slag compositions and additive on heat transfer and crystallization of mold fluxes for high-Al non-magnetic steel. ISIJ Int. 2015;55(5):1000–9.
10. Wu T, Wang Q, He S, Xu J, Long X, Lu Y. Study on properties of alumina-based mold fluxes for high-Al steel slab casting. Steel Res Int. 2012;83(12):1194–202.
11. Xiao D, Wang W, Lu B. Effects of $B_2O_3$ and BaO on the crystallization behavior of $CaO-Al_2O_3$-based mold flux for casting high-Al steels. Metall Mater Trans B. 2015;46(2):873–81.
12. Li Z, You X, Li M, Wang Q, He S, Wang Q. Effect of substituting CaO with BaO and $CaO/Al_2O_3$ ratio on the viscosity of $CaO–BaO–Al_2O_3–CaF_2–Li_2O$ mold flux system. Metals. 2019;9(2):142.
13. Wang Z, Sohn I. Effect of substituting CaO with BaO on the viscosity and structure of $CaO-BaO-SiO_2-MgO-Al_2O_3$ slags. J Am Ceram Soc. 2018;101(9):4285–96.
14. Mascaraque N, Januchta K, Frederiksen KF, Youngman RE, Bauchy M, Smedskjaer MM. Structural dependence of chemical durability in modified aluminoborate glasses. J Am Ceram Soc. 2019;102(3):1157–68.
15. Fernandes HR, Kapoor S, Patel Y, Ngai K, Levin K, Germanov Y, et al. Composition-structure-property relationships in $Li_2O–Al_2O_3–B_2O_3$ glasses. J Non-Cryst Solids. 2018;15(502):142–51.

16. Januchta K, Youngman RE, Goel A, Bauchy M, Rzoska SJ, Bockowski M, et al. Structural origin of high crack resistance in sodium aluminoborate glasses. J Non-Cryst Solids. 2017;15(460):54–65.
17. Bunker BC, Kirkpatrick RJ, Brow RK, Turner GL, Nelson C. Local structure of alkaline-earth boroaluminate crystals and glasses: II, 11B and 27Al MAS NMR spectroscopy of alkaline-earth boroaluminate glasses. J Am Ceram Soc. 1991;74(6):1430–8.
18. Züchner L, Chan JC, Müller-Warmuth W, Eckert H. Short-range order and site connectivities in sodium aluminoborate glasses: I. Quantification of local environments by high-resolution 11B, 23Na, and 27Al solid-state NMR. J Phys Chem B. 1998;102(23):4495–506.
19. Sen S, Xu Z, Stebbins JF. Temperature dependent structural changes in borate, borosilicate and boroaluminate liquids: high-resolution 11B, 29Si and 27Al NMR studies. J Non-Cryst Solids. 1998;226(1–2):29–40.
20. Chan JC, Bertmer M, Eckert H. Site Connectivities in amorphous materials studied by double-resonance NMR of quadrupolar nuclei: high-resolution 11B↔ 27Al spectroscopy of aluminoborate glasses. J Am Chem Soc. 1999;121(22):5238–48.
21. Bertmer M, Züchner L, Chan JC, Eckert H. Short and medium range order in sodium aluminoborate glasses. 2. Site connectivities and cation distributions studied by rotational echo double resonance NMR spectroscopy. J Phys Chem B. 2000;104(28):6541–53.
22. Du LS, Stebbins JF. Site connectivities in sodium aluminoborate glasses: multinuclear and multiple quantum NMR results. Solid State Nucl Magn Reson. 2005;27(1–2):37–49.
23. El Hayek R, Ferey F, Florian P, Pisch A, Neuville DR. Structure and properties of lime alumino-borate glasses. Chem Geol. 2017;461:75–81.
24. Mysen BO, Virgo D, Scarfe CM. Relations between the anionic structure and viscosity of silicate melts—a Raman spectroscopic study. Am Miner. 1980;65(7–8):690–710.
25. Neuville DR, Cormier L, Massiot D. Al environment in tectosilicate and peraluminous glasses: A 27Al MQ-MAS NMR, Raman, and XANES investigation. Geochim Cosmochim Acta. 2004;68(24):5071–9.
26. Massiot D, Fayon F, Capron M, King I, Le Calvé S, Alonso B, et al. Modelling one-and two-dimensional solid-state NMR spectra. Magn Reson Chem. 2002;40(1):70–6.
27. Li JL, Shu QF, Chou K. Effect of $Al_2O_3/SiO_2$ mass ratio on viscosity of $CaO–Al_2O_3–SiO_2–CaF_2$ slag. Ironmaking Steelmaking. 2015;42(2):154–60.
28. Toby BH, Von Dreele RB. GSAS-II: the genesis of a modern open-source all purpose crystallography software package. J Appl Crystallogr. 2013;46(2):544–9.
29. Wu J, Stebbins JF. Effects of cation field strength on the structure of aluminoborosilicate glasses: high-resolution 11B, 27Al and 23Na MAS NMR. J Non-Cryst Solids. 2009;355(9):556–62.
30. Du LS, Stebbins JF. Network connectivity in aluminoborosilicate glasses: a high-resolution 11B, 27Al and 17O NMR study. J Non-Cryst Solids. 2005;351(43–45):3508–20.
31. Angeli F, Charpentier T, De Ligny D, Cailleteau C. Boron speciation in soda-lime borosilicate glasses containing zirconium. J Am Ceram Soc. 2010;93(9):2693–704.
32. Kroeker S, Stebbins JF. Three-coordinated boron-11 chemical shifts in borates. Inorg Chem. 2001;40(24):6239–46.
33. Poe BT, McMillan PF, Cote B, Massiot D, Coutures JP. Structure and dynamics in calcium aluminate liquids: high-temperature 27Al NMR and Raman Spectroscopy. J Am Ceram Soc. 1994;77(7):1832–8.
34. Licheron M, Montouillout V, Millot F, Neuville DR. Raman and 27Al NMR structure investigations of aluminate glasses:(1–x) $Al_2O_3$−xMO, with M= Ca, Sr, Ba and 0.5< x< 0.75. J Non-Cryst Solids. 2011;357(15):2796–801.
35. Duer MJ, editor. Solid state NMR spectroscopy: principles and applications. John Wiley & Sons; 2008, 56-9.
36. Stebbins JF, Kroeker S, Lee SK, Kiczenski TJ. Quantification of five-and six-coordinated aluminum ions in aluminosilicate and fluoride-containing glasses by high-field, high-resolution 27Al NMR. J Non-Cryst Solids. 2000;275(1–2):1–6.
37. Shu Q, Li P, Zhang X, Chou K. Thermodynamics and structure of $CaO-Al_2O_3$-3 mass Pct $B_2O_3$ slag at 1773 K (1500° C). Metall Mater Trans B. 2016;47(6):3527–32.
38. Kim GH, Sohn I. Role of $B_2O_3$ on the viscosity and structure in the $CaO-Al_2O_3-Na_2$ O-based system. Metall Mater Trans B. 2014;45(1):86–95.
39. Li J, Chou K, Shu Q. Structure and viscosity of $CaO–Al_2O_3–B_2O_3$ based mold fluxes with varying $CaO/Al_2O_3$ mass ratios. ISIJ Int. 2020;60(1):51–7.
40. McMillan P, Piriou B, Navrotsky A. A Raman spectroscopic study of glasses along the joins silica-calcium aluminate, silica-sodium aluminate, and silica-potassium aluminate. Geochim Cosmochim Acta. 1982;46(11):2021–37.
41. Neuville DR, Henderson GS, Cormier L, Massiot D. The structure of crystals, glasses, and melts along the $CaO-Al_2O_3$ join: results from Raman, Al L-and K-edge X-ray absorption, and 27Al NMR spectroscopy. Am Miner. 2010;95(10):1580–9.
42. Li JL, Shu QF, Chou KC. Effect of $TiO_2$ addition on viscosity and structure of $CaO–Al_2O_3$ based mold fluxes for high Al steel casting. Can Metall Q. 2015;54(1):85–91.
43. Konijnendijk WL, Stevels J. The structure of borate glasses studied by Raman scattering. J Non-Cryst Solids. 1975;18(3): 307–31.
44. Maniu D, Iliescu T, Ardelean I, Cinta-Pinzaru S, Tarcea N, Kiefer W. Raman study on $B_2O_3–CaO$ glasses. J Mol Struct. 2003;651:485–8.
45. Kamitsos EI, Karakassides MA, Chryssikos GD. Vibrational spectra of magnesium-sodium-borate glasses. 2. Raman and mid-infrared investigation of the network structure. J Phys Chem. 1987;91(5):1073–9.
46. Kamitsos EI, Karakassides MA, Chryssikos GD. A vibrational study of lithium borate glasses with high $Li_2O$ content. Phys Chem Glasses. 1987;28(5):203–9.
47. Yun YH, Bray PJ. B11 nuclear magnetic resonance studies of $Li_2OB_2O_3$ glasses of high $Li_2O$ content. J Non-Cryst Solids. 1981;44(2–3):227–37.
48. Zhong J, Bray PJ. Change in boron coordination in alkali borate glasses, and mixed alkali effects, as elucidated by NMR. J Non-Cryst Solids. 1989;111(1):67–76.
49. Dell WJ, Bray PJ, Xiao SZ. 11B NMR studies and structural modeling of $Na_2O-B_2O_3-SiO_2$ glasses of high soda content. J Non-Cryst Solids. 1983;58(1):1–6.
50. Shanon RDT, Prewitt CT. Effective ionic radii in oxides and fluorides. Acta Crystallogr B. 1969;25:925–46.

51. Shan Z, Liu S, Tao H, Yue Y. Mixed alkaline-earth effects on several mechanical and thermophysical properties of aluminate glasses and melts. J Am Ceram Soc. 2019;102(3):1128–36.
52. Mills KC. The influence of structure on the physico-chemical properties of slags. ISIJ Int. 1993;33(1):148–55.
53. Mills KC. Structure and properties of slags used in the continuous casting of steel: Part 2 specialist mould powders. ISIJ Int. 2016;56(1):14–23.

**How to cite this article:** Singh H, Shu Q, King G, et al. Structure and viscosity of $CaO–Al_2O_3–B_2O_3–BaO$ slags with varying mass ratio of BaO to CaO. *J Am Ceram Soc*. 2021;104:4505–4517. https://doi.org/10.1111/jace.17877